Lattice structures and electronic properties of WZ-$CuInS_2$/WZ-CdS interface from first-principles calculations*

Hong-Xia Liu(柳红霞)[1], Fu-Ling Tang(汤富领)[1,†], Hong-Tao Xue(薛红涛)[1], Yu Zhang(张宇)[1], Yu-Wen Cheng(程育汶)[1], and Yu-Dong Feng(冯煜东)[2]

[1] *State Key Laboratory of Advanced Processing and Recycling of Nonferrous Metals, Department of Materials Science and Engineering, Lanzhou University of Technology, Lanzhou* 730050, *China*

[2] *Science and Technology on Surface Engineering Laboratory, Lanzhou Institute of Physics, Lanzhou* 730000, *China*

(Received 25 April 2016; revised manuscript received 27 August 2016; published online 25 October 2016)

Using the first-principles plane-wave calculations within density functional theory, the perfect bi-layer and monolayer terminated WZ-CIS (100)/WZ-CdS (100) interfaces are investigated. After relaxation the atomic positions and the bond lengths change slightly on the two interfaces. The WZ-CIS/WZ-CdS interfaces can exist stably, when the interface bonding energies are -0.481 J/m^2 (bi-layer terminated interface) and -0.677 J/m^2 (monolayer terminated interface). Via analysis of the density of states, difference charge density and Bader charges, no interface state is found near the Fermi level. The stronger adhesion of the monolayer terminated interface is attributed to more electron transformations and orbital hybridizations, promoting stable interfacial bonds between atoms than those on a bi-layer terminated interface.

Keywords: first-principles calculation, WZ-CIS/WZ-CdS interface, density of states, interface bonding energy, interface states

PACS: 31.15.A–, 75.70.–i, 71.22.+i, 71.15.Nc **DOI:** 10.1088/1674-1056/25/12/123101

1. Introduction

In recent years, the fabrication of pollution-free, low-cost, and high-efficiency photovoltaic cells has attracted successive attention. $CuInS_2$-based thin film has been known as one of the most promising optical absorbers for high-efficiency solar cells.[1,2] It has garnered a great deal of interest due to its high optical absorption coefficient ($> 10^5$ cm^{-1}) higher than conventional III–V semiconductors, desirable band gap (1.45 eV) close to the solar spectra, good thermal property, low cost, environmental, and electrical stability.[3–6] It is reported that $CuInS_2$ (CIS) exists in three polymorphic modifications at different temperatures: the most common and thermodynamically stable chalcopyrite (CP-CIS), metastable zincblende (ZB-CIS), and wurtzite (WZ-CIS) structures.[7,8] It was found that the CIS with the wurtzite structure shows flexibility in stoichiometry, because the copper and indium atoms alternate on the cation site.[9] The wurtzite $CuInS_2$ has been researched in a solar cell device because it provides the ability to tune the Fermi level energy over a wide range, which is beneficial for device fabrication.[10] It has been observed experimentally that this promising material has a high optical absorption coefficient and substantial photo-stability.[9] Because of its strong light absorption over the visible and near-infrared range and good size homogeneity, these nanocrystals were applied as the CIS absorber layer by spraycoating to fabricate working solar cells after the selenization process. The conversion efficiency of CIGS thin film soalr cells was beyond 20%.[11]

Cadmium sulfide (CdS) is a most important II–VI group wide-gap semiconductor with good stability and outstanding optical-electronic properties[12–14] due to its wide energy band gap (2.42 eV)[15] which happens to be in the visible range. CdS have two types of basic structures: the cubic sphalerite and the hexagonal wurtzite.[16] The wurtzite CdS shows novel electronic and optical properties as compared with the sphalerite CdS.[17] Many studies have also reported that the wurtzite CdS nanowires were synthesized in various nanocrystalline forms such as by a simple hydrothermal method.[18] Nowadays, CdS as an efficient *n*-type window material has been widely used in the $CuInS_2$-based thin film solar cell devices.

Thin-film photovoltaic devices were fabricated with a conventional glass/Mo/$CuInS_2$/CdS/ZnO/Al-doped/ZnO configuration.[19] $CuInS_2$ with wurtzite structure is similar to CdS with wurtzite structure. They have the same space group and crystallize as a hexagonal structure. In the processes of preparing solar cells, choosing CIS and CdS with wurtzite structure at the same time, the absorption layer and window layer can make good lattice match, which may reduce the composite effect of the WZ-CIS/WZ-CdS interface. In the WZ-CIS thin film solar cells, the wurtzite $CuInS_2$ nanocrystals

*Project supported by the National Natural Science Foundation of China (Grant Nos. 11164014 and 11364025) and the Gansu Science and Technology Pillar Program, China (Grant No. 1204GKCA057).

†Corresponding author. E-mail: tfl03@mails.tsinghua.edu.cn

© 2016 Chinese Physical Society and IOP Publishing Ltd

were converted with a selenization process, and were applied as the p-type light-absorbing layer in the fabrication. The WZ-CdS window layer is generally deposited on the WZ-CIS absorption layer, which can form the WZ-CIS/WZ-CdS p–n hetero-junction. It is the core part of the WZ-CIS thin film solar cells. The interface between the light-absorbing layer and the window layer is especially important which has greatly influenced the conversion efficiency and performance of the solar cells. Therefore, investigating the interface between WZ-CIS and WZ-CdS gives a systematic understanding to improve CIS solar cell performance and may guide the experiments.

So far, we have performed studies on the CIS solar cells interface: the bond characteristics, electronic structure and interfacial energetic of the Mo (110)/$MoSe_2$ (100) interface,[20] and also for the WZ-CIS (100)/MoS_2 (-100) interface[21] by the first principles calculations. In this work, we theoretically study the properties of bulk WZ-CIS, bulk WZ-CdS, their surfaces and interfaces. For the WZ-CIS/WZ-CdS interface, we investigated two different bond types, and discussed their lattice structures, electronic properties and the interface states at the atomic scale. Furthermore, our results also have been compared with others experimental and calculated results to well understand WZ-CIS solar cells.

2. Methodology

All theoretical calculations were performed within the Vienna ab initio simulation package (VASP)[22–24] with the first principles of density functional theory (DFT). The projector augmented wave (PAW)[25,26] method and the generalized gradient approximations (GGA) functional with the Perdew–Burke–Ernzerhof (PBE)[27] were applied to describe the exchange-correlation energy. We used the pseudopotential for the electronic configurations are [Ar] $3d^{10}4s^1$, [Kr] $5s^25p^1$, [Ne] $3s^23p^4$, and [Kr] $4d^{10}5s^2$, for copper, indium, sulfur, and cadmium, respectively. Γ-centered k-point meshes were applied for bulk WZ-$CuInS_2$, bulk CdS, WZ-$CuInS_2$ surface, WZ-CdS surface, and WZ-CIS/WZ-CdS interface are $11\times11\times7$, $11\times11\times7$, $5\times6\times1$, $5\times6\times1$, and $5\times6\times1$, respectively. We adopted the conjugate gradient (CG) method[28] to optimize atomic structure and selected a cutoff energy of 500 eV based on the plane wave basis. We apply the tetrahedron method with Blöchl corrections[29] for our band structure, density of states and total energy calculations in all systems. Density functional theory (DFT) always underestimates semiconductors' band gaps. In our calculations we added a Hubbard U correction to the GGA energy functional. The values of effective U parameters employed for the 3d states of Cu atoms are 5.5 eV to solve the band gap problem presented in DFT calculations on WZ-$CuInS_2$, which are consistent with other previous studies U-value corrections.[30–32]

3. Results and discussion

3.1. Properties of bulk WZ-$CuInS_2$ and WZ-CdS

To validate the accuracy of the computation methods, we firstly performed calculations on bulks. It is known that Wurtzite $CuInS_2$ (WZ-CIS) belongs to the space group $P63mc$ and crystallizes as a hexagonal wurtzite structure, as shown in Fig. 1(a). Our calculated lattice constants for WZ-$CuInS_2$ are $a = 3.947$ Å, $c = 6.502$ Å, which are matching with other calculated values ($a = 3.90652$ Å, $c = 6.42896$ Å[33]) and experimental values by x-ray diffraction ($a = 3.897$ Å and $c = 6.441$ Å.[34]). Wurtzite CdS also has a hexagonal wurtzite structure with the space group $P63mc$, as shown in Fig. 1(b). Our optimized primitive lattice parameters of $a = 4.17$ Å and $c = 6.76$ Å are in good agreement with other theoretical data ($a = 4.18$ Å, $c = 6.76$ Å[35] and $a = 4.16$ Å, $c = 6.61$ Å[36]) and experimental values ($a = 4.136$ Å, $c = 6.713$ Å[37]), proving the good accuracy of our calculation with a small error limit of 10^{-2} Å. Compared with other data, our calculated values of bulk WZ-CIS and WZ-CdS are in good agreement with other previous reported results.

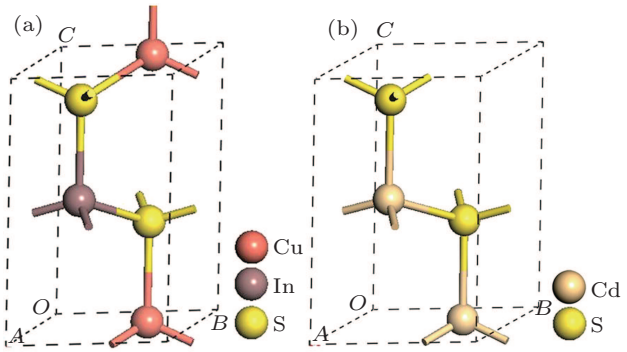


Fig. 1. (color online) The lattice structure of bulk WZ-CIS (a) and bulk WZ-CdS (b).

The band structure and density of states (DOS) were also calculated for bulk WZ-CIS.[21] Through DOS analysis, the WZ-CIS is a direct band gap semiconductor with the calculated band gap of 0.2 eV through the method of GGA + U ($U - J = 5.5$ eV), which is similar with another calculated value[9] but lower than the experimental band gaps (1.47 eV).[38] By analysis of partial density of states (PDOS), the bottom of the conduction band is attributed by 5s-orbital of In atoms, and the uppermost valence band is mainly attributed by 3p-orbital of S atoms.

In WZ-$CuInS_2$, Cu and In atoms randomly locate on the same space group site. At the same time, WZ-$CuInS_2$ has the sub-lattice structure: a tetrahedron containing an S atom at the center and four Cu/In atoms around the S atom. In every tetrahedron, In and Cu atoms may have different site occupancies. There must be five and only five possible occupancies: the S atom is surrounded by two Cu atoms and two In atoms, the S atom is surrounded by three/one In atom(s) and one/three Cu

atom(s), the S atom is surrounded by four Cu/In atoms. The hybrid Hartree–Fock-like functional by Heyd, Scuseria, and Ernzerhof (HSE) can improve the calculation accuracy.[22–24] The first occupancy configuration is the generally used lattice model, which has a band gap 0.86 eV when Hartree–Fock screening parameter $\omega = 0.2$ was employed in HSE06 functional. We also found that WZ-$CuInS_2$ is a semiconductor that may be metallic for different local indium and copper atomic configurations. Metallic configurations have higher lattice energies while semiconductive configurations have lower lattice energies.

Figure 2 shows the band structure and DOS of bulk WZ-CdS. From Fig. 2(a), we found that the WZ-CdS has a direct band gap of 1.2 eV, which is in reasonable agreement with experimental values of 2.48 eV[39] and the other calculated result of 1.22 eV.[40] Figure 2(b) is the calculated DOS of bulk WZ-CdS. The bottom of the conduction band is formed by a mixture of the Cd 5s-orbital and S 3p-orbital, while the top of the valence band is derived from the 3p-orbital of S atoms.

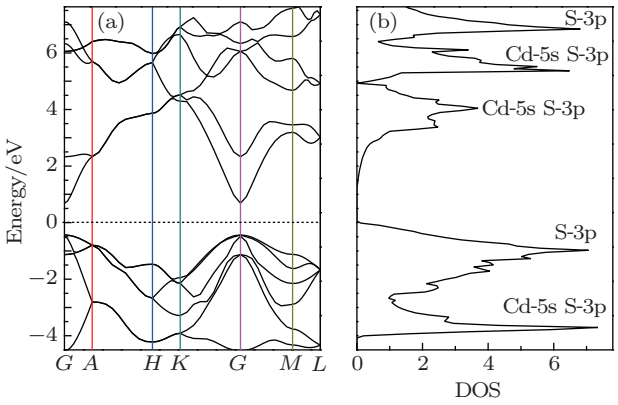


Fig. 2. (color online) The band structure (a) and density of states (b) of bulk WZ-CdS.

3.2. Surface properties

To study the properties of WZ-$CuInS_2$/WZ-CdS interfaces, it is necessary to ensure that both sides of the interface models are thick enough to imitate the bulk. We firstly studied their surface structures. The WZ-$CuInS_2$ (100) surface has two surface models: a bi-layer terminated surface and a monolayer terminated surface. Figures 3(a) and 3(b) show the relaxed lattice structures of the bi-layer terminated and the monolayer terminated WZ-$CuInS_2$ (100) surfaces, respectively. The bi-layer terminated surface model used contains six WZ-CIS bi-layers and the monolayer terminated surface model contains six WZ-CIS bi-layers and one monolayer. The lattice parameters are $a = 7.894$ Å, $b = 6.502$ Å. For the WZ-CdS (100) surface model, there are also bi-layer terminated (contains six WZ-CdS bi-layers) and monolayer terminated (contains six WZ-CdS bi-layers and one monolayer) surface models. Figures 3(c) and 3(d) show the lattice structures of bi-layer terminated and monolayer terminated WZ-CdS (100) surfaces after relaxation respectively. The lattice parameters are $a = 8.340$ Å, $b = 6.760$ Å. For all our surface models, we fixed the two bottom layers, and also applied a 25-Å thickness vacuum region to avoid the effect of periodic boundary conditions.

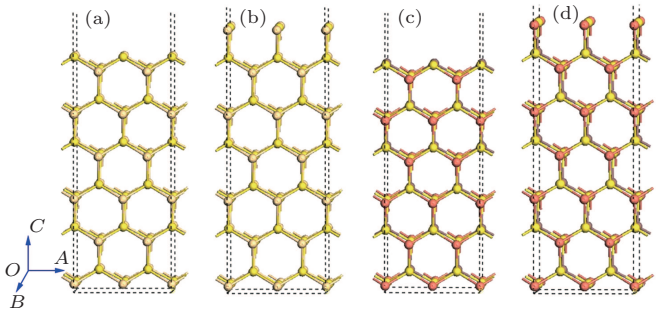


Fig. 3. (color online) The lattice structure of relaxed bi-layer terminated (a) and monolayer terminated (b) WZ-CuInS2 (100) surface; the lattice structure of relaxed bi-layer terminated (c) and monolayer terminated (d) WZ-CdS (100) surface.

The stability of a surface can be described via the surface energy. The surface energy γ[41] is obtained from a slab including two identical surfaces, through Eq. (1):

$$\gamma = \frac{1}{2A}\left(E_{\text{slab}} - \frac{N_{\text{s}}}{N_{\text{b}}}E_{\text{bulk}}\right), \tag{1}$$

where E_{slab} and E_{bulk} denote the total energy of a slab and a bulk unit, N_{s} and N_{b} represent the amount of atoms in the slab and bulk unit, respectively, A represents the unit surface area, and the factor 1/2 means that there are two identical surfaces in one slab. The calculated WZ-$CuInS_2$ (100) surface energies for the bi-layer terminated surface is 0.84 J/m^2 and for the monolayer terminated surface is 1.07 J/m^2. It shows that the bi-layer terminated WZ-$CuInS_2$ (100) surface is predicted to be the more stable structure in terms of energetic favorability. For our bi-layer terminated and monolayer terminated WZ-CdS (100) surface models the calculated surface energies are 0.46 J/m^2 and 0.77 J/m^2, respectively. It also means that the bi-layer terminated WZ-CdS (100) surface is more stable than the monolayer terminated surface. Then, we examined the interlayer spacing change for two WZ-$CuInS_2$ (100) surface slabs after relaxation. We found that the interlamellar spacing contraction/expansion is at the range of 0.001 Å–0.004 Å. It seems that there is almost no change between the interior layers after optimization. Similarly, we also checked the two relaxed WZ-CdS (100) surface slabs by calculating the interlayer spacing. We found that the interlamellar spacing contraction/expansion is at the range of 0.001 Å–0.005 Å. It means that there is a very small change between the interior layers: the biggest contraction/expansion mainly takes place in the first layer. When the surface model is thick enough the interior layers can exhibit the bulk-like characters. From the interlayer spacing changes

it exhibits that our model slabs are sufficient to imitate the feature of the bulk. Through the above analysis it reveals that for both WZ-$CuInS_2$ (100) and WZ-CdS (100) surfaces the interlayer relaxations in monolayer terminated surfaces are larger than that in the bi-layer terminated surfaces. Compared with our calculated interlayer spacing values, which implies that the bi-layer terminated surfaces are more stable than the monolayer terminated surfaces. This result agrees well with our calculated surface energy.

We have also obtained the electronic properties for the surfaces. Through analysis of the local density of states (LDOS) of WZ-CIS (100) and WZ-CdS (100) surfaces we found that no new electronic states appeared near the Fermi level, which means that there is no existence of surface states on the surfaces.

3.3. Structure and electronic properties of WZ-$CuInS_2$ (100)/WZ-CdS (100) interface

3.3.1. Interface geometry of WZ-$CuInS_2$/WZ-CdS

Building the WZ-$CuInS_2$/WZ-CdS interface model for simulation needs good surface lattice matching. We find that WZ-$CuInS_2$ (100) and WZ-CdS (100) faces can make a good lattice matching, and the lattice mismatch between two slabs is less than 5.6%, as shown in Fig. 4. For WZ-CdS (100) and WZ-$CuInS_2$ (100) planes, we find that there are in existence two bonding styles (A and B bonding styles) while building the interface model. As Figs. 5(a) and 6(b) show, they are bi-layer faced to bi-layer and monolayer faced to monolayer on the interface, respectively. We studied both of them.

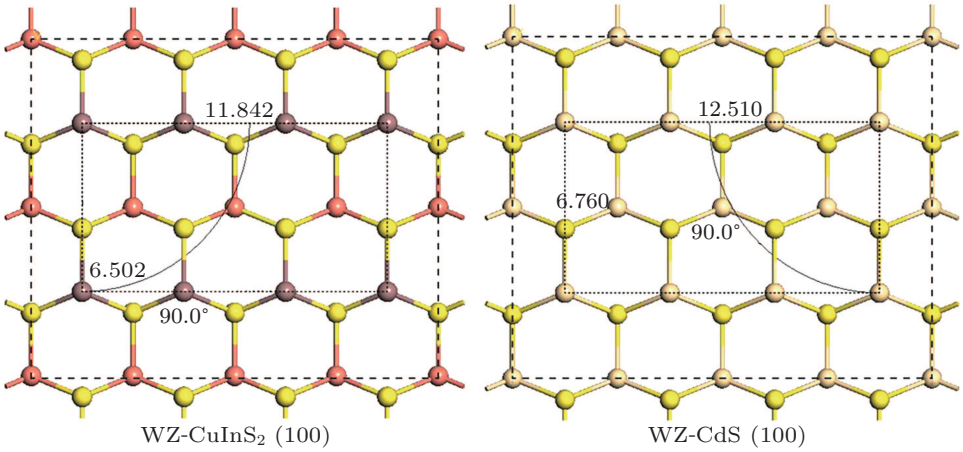


Fig. 4. (color online) The lattice mismatch of the WZ-CIS (100)/WZ-CdS (100) interface (the lattice parameters have the unit of Å).

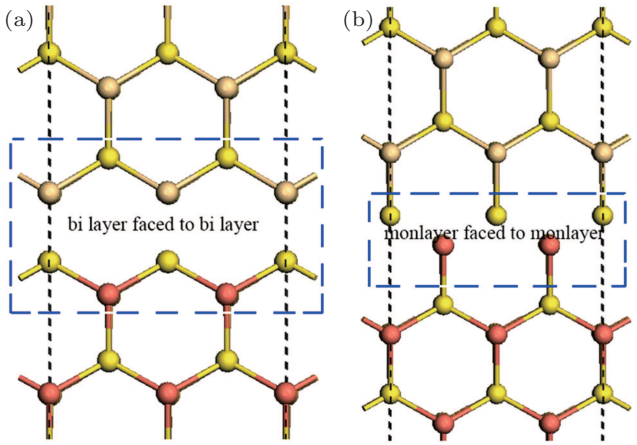


Fig. 5. (color online) The two interface bonding styles: (a) bi-layer faced to bi-layer on the interface (model A); (b) monolayer faced to monolayer on the interface (model B).

Based on the above calculations, we build the WZ-$CuInS_2$/WZ-CdS interface models for DFT computations and studied their local lattice structure and electronic properties through the interface models (Fig. 6). For our interface models, we added some hydrogen atoms on WZ-CIS and WZ-CdS surfaces to passivate those surface dangling bonds to eliminate the influence of dangling bonds on the left (WZ-CIS) and the right (WZ-CdS) surfaces. In interface model A (shown in Fig. 6(a)) which is the bi-layer terminated surface faced to the bi-layer terminated surface on the interface (called the bi-layer terminated interface for short), the left part has six bi-layers of WZ-$CuInS_2$ (100) planes, and the right part has six bi-layers of WZ-CdS (100) planes. It contains 104 atoms, including 12 Cu, 12 In, 24 Cd, 48 S, and 15 H atoms. In interface model B (Fig. 6(b)) which is the monolayer terminated surface faced to the monolayer terminated surface on the interface (called the monolayer terminated interface for short), the left part has one monolayer, six bi-layers of WZ-CIS (100) planes, the right part has one monolayer, six bi-layers of WZ-CdS (100) planes. It contains 112 atoms, including 14 Cu, 12 In, 26 Cd, 52 S, and 8 H atoms. The lattice parameters in interface models A and B are $a = 8.117$ Å, $b = 6.631$ Å. For our interface models A and B we add both a 30-Å thickness vacuum region to avert the interactions between the slab and its images. A suitable interface distance is acquired through the single point energy calculations method. We can seek the lowest total energy of

the interface system through changing the interfacial interlayer distance. After testing ten sets of data, we find that when the distance is 2.380 Å for the bi-layer terminated interface (as shown in Fig. 6(c)) and 1.527 Å for the monolayer terminated interface (as shown in Fig. 6(d)), the interface atoms have the smallest calculated stress. In order to better study the interfacial properties, we fixed the left three bi-layers on the WZ-CIS part, the right three bi-layers on the WZ-CdS part in both of the bi-layer terminated and monolayer terminated interface models.

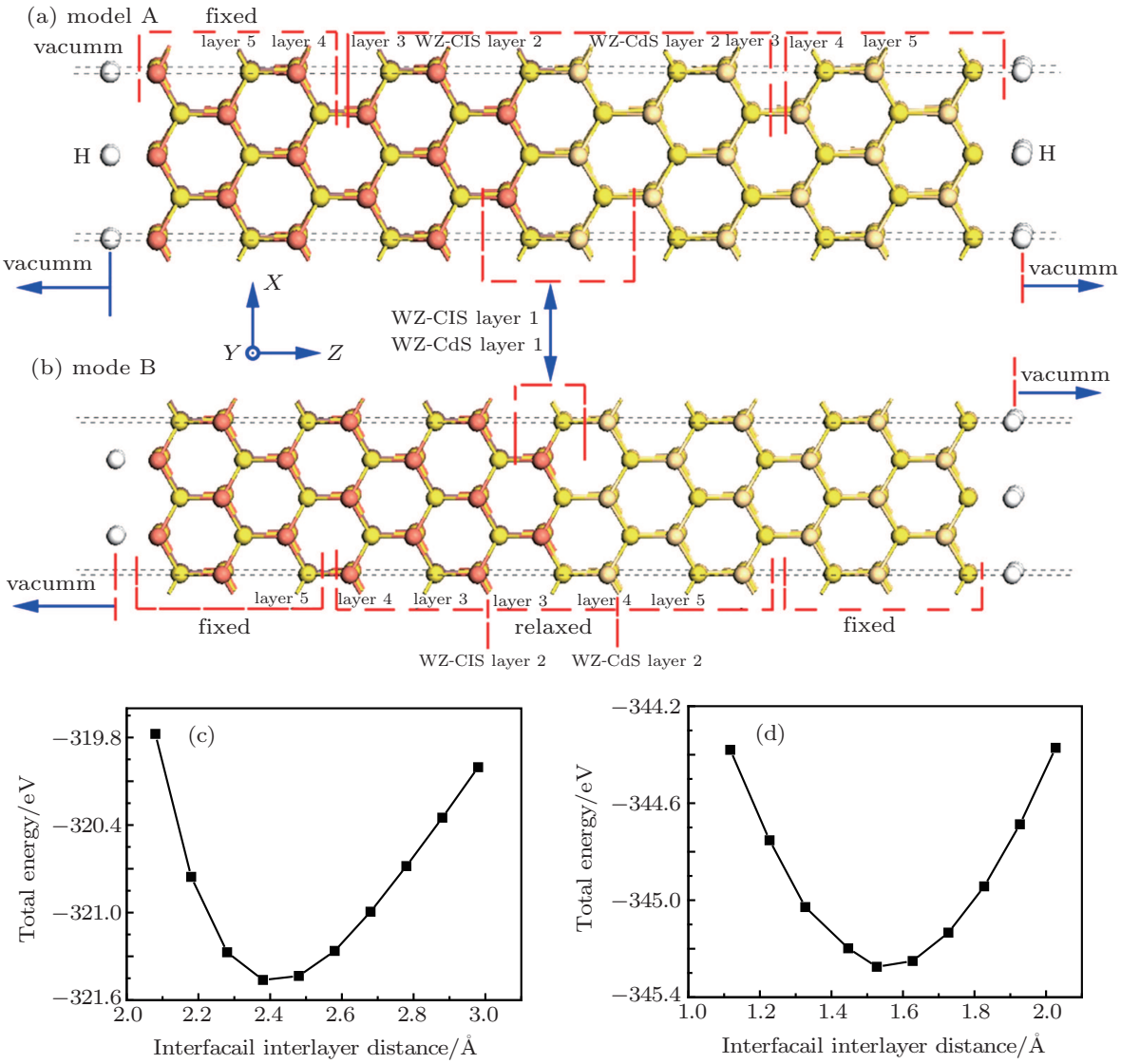


Fig. 6. (color online) WZ-CIS (100)/WZ-CdS (100) interface model: (a) bi-layer terminated interface (model A) and (b) monolayer terminated interface (model B); the total energy dependence on the bi-layer terminated interface distance (c), and monolayer terminated interface distance (d).

The atoms positions and bond lengths change before and after relaxation for bi-layer terminated and monolayer terminated WZ-CIS (100)/WZ-CdS (100) interfaces are shown in Fig. 7. We found that the positions and the bond lengths of atoms changed a little near the interface. For the bi-layer terminated interface model, comparing the atoms positions and bond lengths before relaxation (Fig. 7(a)) and after relaxation 7(b) near the interface, we found that the atomic positions have little changes along the direction of c, while there is almost no atomic position change in directions a and b. After relaxation the bond lengths $d_{\mathrm{Cd-S}}$ are 2.521 Å, $d_{\mathrm{In-S}}$ are 2.492 Å on the interface, while before relaxation $d_{\mathrm{Cd-S}}$, $d_{\mathrm{In-S}}$ are 2.520 Å; after relaxation the bond lengths $d_{\mathrm{Cd-S}}$ are 2.535 Å–2.573 Å, $d_{\mathrm{Cu-S}}$ are 2.286 Å–2.347 Å, $d_{\mathrm{In-S}}$ are 2.286 Å–2.561 Å near the interface, while before relaxation $d_{\mathrm{Cd-S}}$ are 2.501 Å–2.546 Å, $d_{\mathrm{Cu-S}}$, $d_{\mathrm{In-S}}$ are 2.425 Å–2.471 Å. We can see that after relaxation the bond lengths $d_{\mathrm{Cd-S}}$, $d_{\mathrm{In-S}}$ have a trend of elongation while $d_{\mathrm{Cu-S}}$ have some contraction. For the monolayer terminated interface model, we also compared the atoms positions and bond lengths before (Fig. 7(c)) and after (d) structural relaxation near the interface. Seen from Fig. 7(d), we can find that after relaxation the atoms on the interface have certain small degrees of movement. After relaxation the bond lengths $d_{\mathrm{Cd-S}}$ are 2.592 Å, $d_{\mathrm{Cu-S}}$ are 2.294 Å, while before relaxation $d_{\mathrm{Cd-S}}$ and $d_{\mathrm{Cu-S}}$ are 2.471 Å on the interface; after relaxation the bond lengths $d_{\mathrm{Cd-S}}$ are 2.539 Å–2.551 Å, $d_{\mathrm{Cu-S}}$

are 2.316 Å–2.397 Å, $d_{\mathrm{In-S}}$ are 2.316 Å–2.424 Å near the interface, while before relaxation $d_{\mathrm{Cd-S}}$ are 2.501 Å–2.546 Å, $d_{\mathrm{In-S}}$ and $d_{\mathrm{Cu-S}}$ are 2.425 Å–2.471 Å. Comparing Fig. 7(b) with Fig. 7(d), we found that after relaxation the positions and bond lengths of the atoms near the interface have small changes on the two interface models. But the monolayer terminated interface has even larger position changes than those on the bi-layer terminated interface, we can infer that the structure of the bi-layer terminated interface is relatively more stable than the monolayer terminated interface.

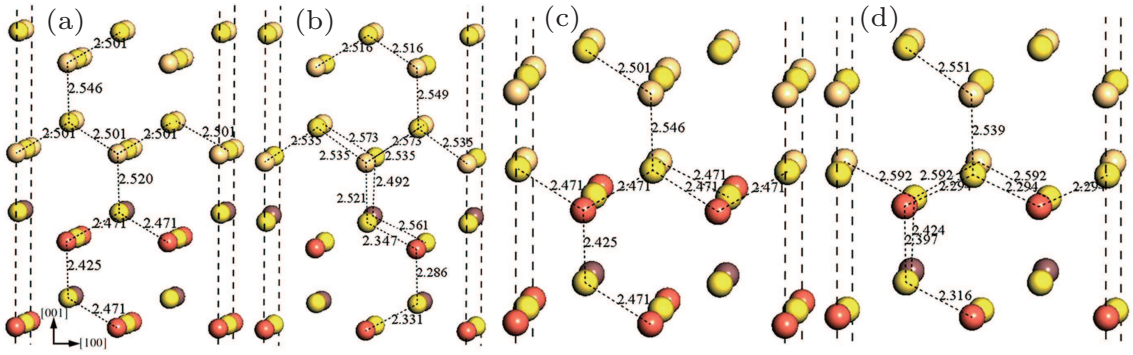


Fig. 7. (color online) The atoms positions and bond lengths changes of the bi-layer terminated WZ-CIS (100)/WZ-CdS (100) interface before (a) and after (b) relaxation near the interface; the atoms positions and bond lengths changes of the monolayer terminated interface before (c) and after (d) relaxation near the interface.

3.3.2. Interface adhesion energies

Adhesion energy is the key factor to predict interfacial bonding stability.[42] We calculated the interface bonding energy to qualitatively analyze the interface combination stability of two different models. A negative bonding energy means a stable interface structure.[43] We use Eq. (2) to calculate WZ-CIS (100)/ WZ-CdS (100) interface bonding energy,

$$E_{\mathrm{ads}}\,(\mathrm{eV/\AA^2}) = [E_{\mathrm{WZ-CIS/CdS}}\,(\mathrm{eV}) - E_{\mathrm{WZ-CIS}}\,(\mathrm{eV}) - E_{\mathrm{CdS}}\,(\mathrm{eV})]/2A, \quad (2)$$

where $E_{\mathrm{WZ-CIS/MoS2}}$ is the total energy of the WZ-CIS/WZ-CdS interface. $E_{\mathrm{WZ-CIS}}$, $E_{\mathrm{WZ-CdS}}$ are the total energy of individual WZ-CIS (100) and WZ-CdS (100) slabs in the same supercell respectively. When we calculated $E_{\mathrm{WZ-CIS}}$ or $E_{\mathrm{WZ-CdS}}$, one part of the interface system is fixed, and the other part is removed (A is the interface area). Here, the interface bonding energy we calculated for the WZ-CIS/WZ-CdS model A is -0.481 J/m^2, and that for model B is -0.677 J/m^2. Firstly, those negative bonding energies mean that the WZ-CIS/WZ-CdS interfaces can exist stably with a stronger bonding ability. Then, comparing the E_{ads} of the two interface models with each other, the bi-layer terminated interface structure (interface model A) has a larger value of E_{ads} than that of the monolayer terminated ones (interface model B). So we can infer that the monolayer terminated interface has a stronger bonding ability. Usually, the interfacial bonding characteristic acts a crucial role to predict the mechanical properties of an interface.

3.3.3. Electronic properties of WZ-CIS/WZ-CdS interface

In order to further explore the bonding ability of the interface, we studied the local density of states (LDOS) and the partial density of states (PDOS), interfacial difference charge density distribution, Bader charges are calculated both for the bi-layer terminated (interface model A) and monolayer terminated (interface model B) WZ-CIS/WZ-CdS interfaces.

The local density of states (LDOS) and partial density of states (PDOS) of WZ-CIS/WZ-CdS interfaces were shown in Fig. 8. Figure 8(a) shows the bi-layer terminated interface local density of states. We can see that there are no obvious interface states near the Fermi level, only a small density peak at 0.75 eV both in WZ-CIS layer 1 and WZ-CdS layer 1 on the interface. We also find that the band gap has some offsets which the valence band moves far away from the Fermi level and the conduction band moves close to the Fermi level on the interfacial. Comparing the LDOS of the internal layers from layer 5 to layer 1 of the WZ-CIS part, we find that some electrons transfered from the high energy level to low energy level, especially at the position of 0 eV to -5 eV, and the same condition also arises on WZ-CdS parts. Figure 8(b) shows the monolayer terminated interface local density of states. We can see that there exists a very small density peak on the Fermi level in WZ-CdS layer 1. On the interface the band gap of WZ-CIS and WZ-CdS parts also have some offsets: the valence band moves close to the Fermi level, which has the opposite appearance compared with LDOS of the bi-layer terminated interface (in Fig. 8(a)). Comparing the LDOS of the internal layers from layer 5 to layer 1 of WZ-CIS and WZ-CdS parts, we find that the electrons have a little transfer from the low energy level to the high energy level at the position of -5 eV to 0 eV. We can conclude that there are almost no newly appeared interface states near the Fermi level for two WZ-CIS/WZ-CdS interface bonding styles, which is in favor of the electrical conductivity of the WZ-CIS/WZ-CdS p–n hetero-junction and beneficial to the conversion efficiency of solar cells.

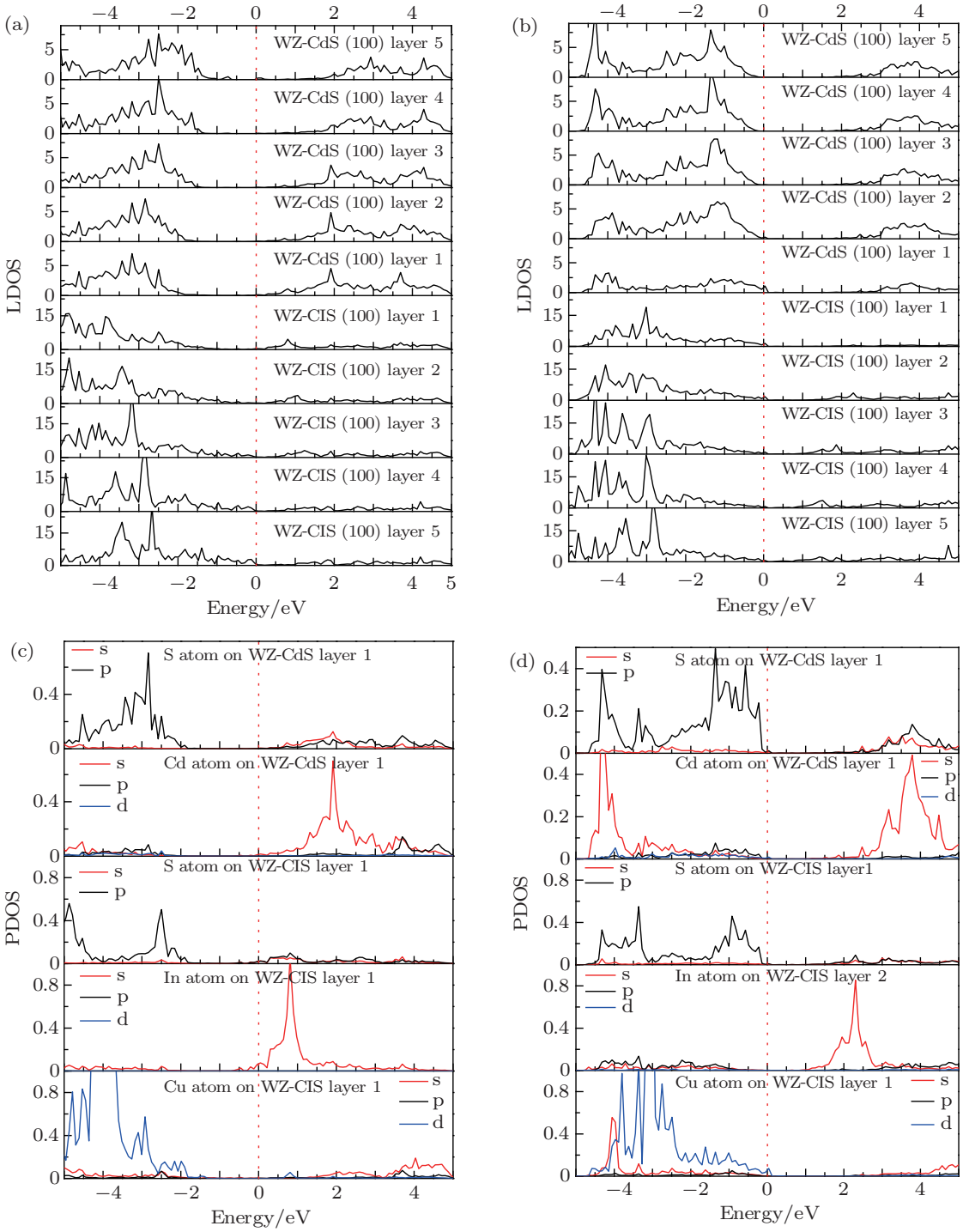


Fig. 8. (color online) The local density of states (LDOS) of bi-layer terminated (a) and monolayer terminated (b) WZ-CIS (100)/WZ-CdS (100) interface; (c) the partial density of states (PDOS) of Cu, In, S atoms in WZ-CIS layer 1 and Cd, S atoms in WZ-CdS layer 1 for the bi-layer terminated interface model; (d) the PDOS of Cu, S atoms in WZ-CIS layer 1, In atom (in WZ-CIS layer 2), and Cd, S atoms in WZ-CdS layer 1 for the monolayer terminated interface model.

Figure 8(c) is the PDOS in the bi-layer terminated interface for Cu, S, In atoms in WZ-CIS layer 1, and for Cd, S atoms in WZ-CdS layer 1. Figure 8(d) is the PDOS of the monolayer terminated interface for Cu, S, atom in WZ-CIS layer 1, In atoms in WZ-CIS layer 2, and for Cd, S atoms in WZ-CdS layer 1. From Fig. 8(c) we find that the S-3p orbital of WZ-CdS has a hybridization with the Cu-3d orbital of WZ-CIS from −5.0 eV to −2.0 eV, and also a hybridization of S-3p orbital of WZ-CdS with Cu-3s orbital of WZ-CIS from 2.0 eV to 5.0 eV; a little hybridization of the S-3p orbital of WZ-CdS with In-5s of WZ-CIS at about 0.5 eV to 4.0 eV; the Cd-5s orbital of WZ-CdS with S-3p orbital of WZ-CIS has a small hybridizations at about 0.2 eV to 4.5 eV. These hybridizations will improve the bonding ability between Cu and S, Cd and S, S and In atoms on the interface.

From Fig. 8(d), we can see that the S-3p orbital of WZ-CdS has a strong hybridization with the Cu-3d orbital of WZ-CIS from −4.5 eV to 0 eV, especially the S-3p orbital of WZ-

CdS has a large hybridization with the Cu-4s orbital of WZ-CIS near the position of −4 eV. Those orbital hybridizations enhance the Cu-S bond on the interface. The Cd-5s orbital of WZ-CdS with the S-3p orbital of WZ-CIS also has a hybridization at about −4.8 eV to −0.1 eV, which promoted the bonding of Cd–S on the interface.

By comparing Fig. 8(c) with 8(d), we find that for the monolayer terminated interface the orbital hybridizations ability between interfacial atoms are stronger than those in the bi-layer terminated interface, which results in a relatively stable adhesion of the interface ($E_{ads} = -0.677$ J/m^2). The bonding between the Cd–S and Cu–S in the interface area reveals that the monolayer terminated interface is stronger than the bi-layer terminated interface. It can be concluded that the interaction between the Cd–S and Cu–S is the dominant factors determining the adhesion strength between WZ-CIS and WZ-CdS. Hence, the adhesion of the monolayer terminated interface is stronger and stabler than that in the bi-layer terminated interface.

We also calculated the difference charge density for two interface bonding styles of WZ-CIS/WZ-CdS to further clarify their interfacial bonding and electronic structure. The difference charge density ρ is defined in Eq. (3):

$$\rho = \rho_{\mathrm{WZ-CIS/WZ-CdS}} - \rho_{\mathrm{WZ-CIS}} - \rho_{\mathrm{WZ-CdS}}. \tag{3}$$

In Eq. (3), $\rho_{\mathrm{WZ-CIS/WZ-CdS}}$ represents the total charge density of the interface systems, $\rho_{\mathrm{WZ-CIS}}$ and $\rho_{\mathrm{WZ-CdS}}$ represent the isolated WZ-CIS slabs and WZ-CdS slabs of the same systems respectively.

Figure 9 shows the difference charge densities of the bi-layer terminated and monolayer terminated interfaces. Figures 9(a) and 9(c) provide the general charge transfer in the bi-layer terminated and the monolayer terminated interface systems, respectively. Figures 9(b) and 9(d) are the partial enlarged views corresponding with Figs. 9(a) and 9(c) (the green areas mean positive, and the purple areas mean negative ρ). From Fig. 9, we can see that on the interface there are obvious accumulated charge region, revealing that the electrons are largely redistributed on the interface. This electron transfer can promote the bonding between the interfacial atoms.

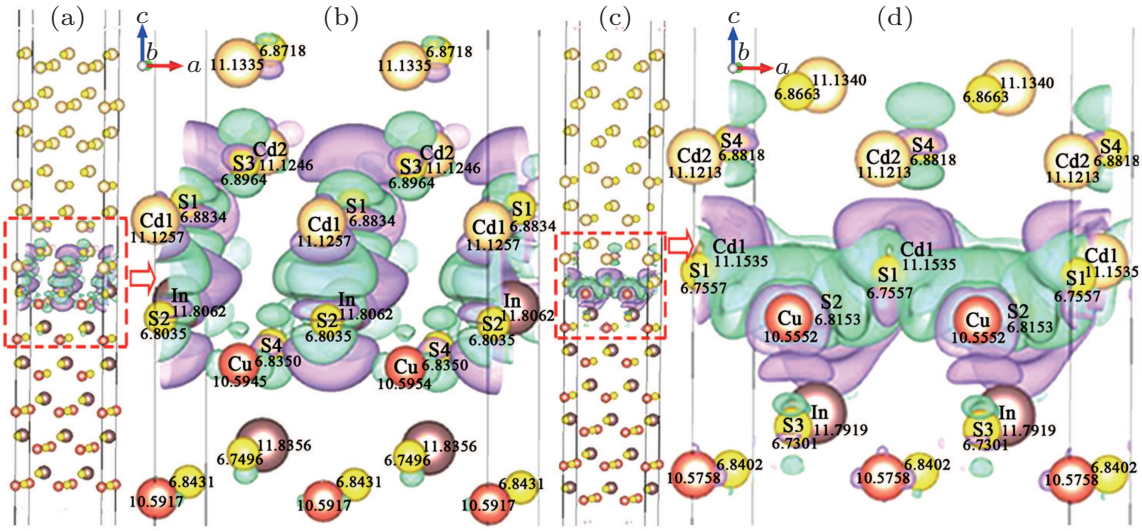


Fig. 9. (color online) The general Charge density difference (a) and partial enlarged view (b) (including Bader charges) for model A interface; the general charge density difference (c), and partial enlarged view (d) (including Bader charges) for model B interface.

For the bi-layer terminated interface, seen from Figs. 9(a) and 9(b), the electrons redistribute on the interface layers of WZ-CdS layer 1 and WZ-CIS layer 1. The number of the electrons between three Cd1 and three S3, three S1 and three Cd2 atoms reduces. On the opposite WZ-CIS side, we also found that the electron reductions between three S2 and two Cu, three In and two S4 atoms. Those reduced electrons are largely transfered to the area between Cd1 and S2, S1 and In atoms, which promoted bonding between the interfacial of Cd1 and S2, S1 and In atoms. For the monolayer terminated interface, seen from Figs. 9(c) and 9(d), the charge also highly accumulates on the interface region, which proved the formation of stronger bonding between the interfacial atoms. On the other hand, the electron transfers from their adjacent Cu and S3, S2 and In1 atoms of WZ-CIS side to the interfacial area among the S1 and Cu, Cd1 and S2 atoms. Moreover, the numbers of the electrons between interfacial Cd1 and S1 atoms of WZ-CdS side transfer to the interface, and same conditions occur between the interfacial Cu and S2 atoms of WZ-CIS side, suggesting that these reduced electrons highly promote the bonding of Cd–S and S–Cu on the interface. By comparing Fig. 9(b) with 9(d), we found that the adhesion of the monolayer terminated interface is stronger, attributing to more electron transfers to the interface region, which is in favour of formation stable interfacial bonding.

Table 1. Bader charges of bulk WZ-CIS and WZ-CdS, WZ-CIS and WZ-CdS surfaces in interface models A and B, respectively. The unit of Bader charges is electrons (e).

Systems	Charges of Cu	Charges of In	Charges of S	Charges of Cd
Bulk WZ-CIS	10.5128	11.8528	6.8069-6.8274	
WZ-CIS (interface model A)	10.5659-10.6289	11.7137–11.8356	6.7166-6.8431	
WZ-CIS (interface model B)	10.5552-10.6077	11.7037–11.7919	6.7227-6.8402	
Bulk WZ-CdS			6.8782	11.1218
WZ-CdS (interface model A)			6.8718–6.9084	11.0906–11.1335
WZ-CdS (interface model B)			6.7497–6.9106	11.0893–11.1535

Their Bader charges are also analyzed, to further clarify their electronic properties of bi-layer terminated and monolayer terminated interfaces. We marked the atomic charges near the interface in Figs. 9(b) and 9(c). Table1 shows the Bader charges of the bulk compared with those on the interfaces. For the bi-layer terminated interface, we found that on the WZ-CdS side the Cd1 and Cd2 atoms get fewer charges (about 0.003–0.004), while the S1 and S3 atoms get some charges (about 0.01–0.02). On the opposite WZ-CIS side, the In atoms lose some charges (about 0.05), and the Cu atoms get more charges (about 0.08), while the S2 and S4 atoms get little charges (about 0.01–0.03). For the monolayer terminated interface, the Cd1 atoms get little charges (about 0.03), and the S1 atoms lose much more charges (about 0.17). On the WZ-CIS side, the Cu atoms get some charges (about 0.04), the S2 atoms lose little charges (about 0.01), and the adjacent In and S3 atoms also lose some charges (about 0.06 and 0.07). From the above analysis, we can conclude that the monolayer terminated interface gains or loses more charges on the interface, which inferred that the bonding of this interface is more stable. These results also correspond well with our partial density of states and difference charge density results.

From the above analysis, we can infer that the WZ-CIS/WZ-CdS interface has better stability, and no interface states appeared on the interface, which is beneficial to the conductivity of WZ-CIS based solar cells. Also, after investigating the bi-layer and monolayer terminated WZ-CIS (100)/WZ-CdS (100) interfaces, we found that the bonding style of the monolayer terminated interface has a more strong adhesion ability and stability than the bi-layer terminated interface. It is attributed to more electron transformations and orbital hybridizations on the interface promoting formation of the stable interfacial bonds, which is also beneficial to improving the conversion efficiency of solar cells.

4. Conclusions

In conclusion, we used the first-principles calculations to study WZ-CIS (100)/WZ-CdS (100) interfaces, including the interface structure, adhesion energy, interfacial bonding and electronic properties. Considering bi-layer terminated and monolayer terminated bonding styles, the main findings are as follows.

(i) The WZ-CIS (100) and WZ-CdS (100) surfaces have a lattice mismatch of 5.6%.

(ii) After relaxation the atoms position and bond lengths have changed slightly on the interface.

(iii) The interface binding energy we calculated for the bi-layer terminated interface is -0.481 J/m^2, and that for the monolayer terminated interface is -0.677 J/m^2, indicating that the WZ-CIS/WZ-CdS interface can bond well and also the latter system has better stability.

(iv) There are almost no newly appeared interface states near the Fermi level for two WZ-CIS/WZ-CdS interface bonding styles, which are in favor of the electrical conductivity of WZ-CIS/WZ-CdS p–n heterojunction, and are beneficial to the conversion efficiency of solar cells.

(v) The interfacial orbital hybridizations enhance the bonding of the interface.

(vi) The electrons of atoms transfer on the interfaces promote the bonding between atoms and increase the interface adhesion. The adhesion of the monolayer terminated interface is faster, attributing to more electrons transferring to the interface region, and the formation of more stable interfacial bonding than the bi-layer terminated interface.

Acknowledgements

This work was performed in the Gansu Supercomputer Center.

References

[1] He Y B, Kriegseis W, Meyer B K, Polity A and Serafin M 2003 *Appl. Phys. Lett.* **83** 1743
[2] Wätjen J T, Scragg J J, Ericson T, Edoff M and Platzer-Björkman C 2013 *Thin Solid Films* **535** 31
[3] Bandyopadhyaya S, Chaudhuri S and Pal A K 2000 *Sol. Energy Mater. Sol. Cells* **60** 323
[4] Klaer J, Bruns J, Henninger R, Siemer K, Klenk R, Ellmer K and Bräunig D 1998 *Semicond. Sci. Technol.* **13** 1456
[5] Wang Z D, Mo X L, Li J, Sun D L and Chen G R 2009 *J. Alloys Compd.* **487** L1
[6] Heidemann F, Gutay L, Meeder A and Bauer G H 2009 *Thin Solid Films* **517** 2427
[7] Gusain M, Kumar P and Nagarajan R 2013 *RSC Adv.* **3** 18863
[8] Yin Z, Hu Z L, Ye H H, Teng F, Yang C H and Tang A W 2014 *Appl. Surf. Sci.* **307** 489
[9] Tomi S, Bernasconi L, Searle B G and Harrison N M 2014 *J. Phys. Chem. C* **118** 14478

[10] Sheng X, Wang L, Luo Y P and Yang D R 2011 *Nanoscale Res. Lett.* **6** 562
[11] Jackson P, Hariskos D, Lotter E, Paetel S, Wuerz R, Menner R, Wischmann W and Powalla M 2011 *Prog. Photovoltaics* **19** 894
[12] Priyam A, Chatterjee A, Bhattacharya S C and Saha A 2007 *J. Cryst. Growth* **304** 416
[13] Barnham K, Marques J L, Hassard J and O'Brien P 2000 *Appl. Phys. Lett.* **76** 1197
[14] Cao H Q, Wang G Z, Zhang S C, Zhang X R and Daniel R 2006 *Inorg. Chem.* **45** 5103
[15] Shafaay B A 2014 *J. Chem. Bio. Phy. Sci. Sec. C* **4** 3606
[16] Xiong Y S, Zhang J, Huang F, Ren G Q, Liu W Z, Li D S, Wang C and Lin Z 2008 *J. Phys. Chem. C* **112** 9229
[17] Ninomiya S and Adachi S 1995 *J. Appl. Phys.* **78** 1183
[18] Pan A L, Wang S Q, Liu R B, Li C R and Zou B S 2005 *Small* **11** 1058
[19] Huang W C, Tseng C H, Chang S H, Tuan H Y, Chiang C C, Lyu L M and Huang M H 2012 *Langmuir* **28** 8496
[20] Liu H X, Tang F L, Xue H T, Zhang Y and Feng Y D 2015 *Appl. Surf. Sci.* **351** 382
[21] Zhang Y, Tang F L, Xue H T, Lu W J, Liu J F and Huang M 2015 *Physica E* **66** 342
[22] Kresse G and Furthmüller J 1996 *Comp. Mater. Sci.* **6** 15
[23] Kresse G and Furthmüller J 1996 *Phys. Rev. B* **54** 11169
[24] Yu J, Lin X, Wang J J, Chen J and Huang W D 2009 *Appl. Surf. Sci.* **255** 9032
[25] Ma L C, Zhang J M and Xu K W 2013 *Physica E* **50** 1
[26] Kresse G and Joubert D 1999 *Phys. Rev. B* **59** 1758
[27] Perdew J P, Burke K and Ernzerhof M 1996 *Phys. Rev. Lett.* **77** 3865
[28] Zhou J G, Causon D M, Mingham C G and Ingram D M 2001 *J. Comput. Phys.* **168** 1
[29] Blöchl P E, Jepsen O and Andersen O K 1994 *Phys. Rev. B* **49** 16223
[30] Hinuma Y, Oba F, Kumagai Y and Tanaka I 2013 *Phys. Rev. B* **88** 035305
[31] Liechtenstein A L, Anisimov V L and Zaanen J 1995 *Phys. Rev. B* **52** 5467
[32] Lany S and Zunger A 2005 *Phys. Rev. B* **72** 035215
[33] Qi Y X, Liu Q C, Tang K B, Liang Z H, Ren Z B and Liu X M 2009 *J. Phys. Chem. C* **113** 3939
[34] Pan D C, An L J, Sun Z M, Hou W, Yang Y, Yang Z Z and Lu Y F 2008 *J. Am. Chem. Soc.* **130** 5620
[35] Knudson M D, Gupta Y M and Kunz A B 1999 *Phys. Rev. B* **59** 11704
[36] Grünwald M, Zayak A, Neaton J B, Geissler P L and Rabani E 2012 *J. Chem. Phys.* **136** 234111
[37] Xue H G, Shen Z Q and Li C M 2005 *Biosens. Bioelectron.* **20** 2330
[38] Zhou F F, Chen Q M, Chen J, Wang T T, Jia Z, Dou X M and Zhuang S L 2014 *Opt. Instrum.* **36** 342
[39] Madelung O 2004 *Semiconductors: data handbook* (New York: Springer) p. 289
[40] Deng H X, Li S S, Li J B and Wei S H 2012 *Phys. Rev. B* **85** 195328
[41] Wang B D, Dai J H, Wu X, Song Y and Yang R 2015 *Intermetallics* **60** 58
[42] Siegel D J, Hector L G and Adams J B 2002 *Surf. Sci.* **498** 321
[43] Lu Z S, Li S S, Chen C and Yang Z X 2013 *Acta. Phys. Sin.* **62** 117301 (in Chinese)